Submitted to the
XXI International Symposium on Lepton and Photon Interactions at High Energies
11-16 August 2003 Fermi National Accelerator Laboratory, Batavia, Illinois USA

Abstract:

Measurement of the proton structure functions F_2 and F_L using initial state radiative events at HERA

ZEUS Collaboration

Abstract

The first direct measurement at HERA of the longitudinal proton structure function, F_L, has been made using the ZEUS detector. The measurement technique exploits the variation of the lepton beam energy in events in which a hard initial state photon is emitted. The photon was detected in the luminosity monitor. This class of events was also used to make measurements of the structure function F_2 in the kinematic range $0.3 < Q^2 < 22\,\mathrm{GeV}^2$ and $8\times10^{-6} < x < 1.8\times10^{-1}$. These data cover the region between previous F_2 measurements at HERA and those made at fixed target experiments. Both structure function measurements are compared to next-to-leading-order perturbative QCD as implemented in the DGLAP evolution equations.

1 Introduction

Measurements of the proton structure function, F_2, in neutral current (NC) deep inelastic scattering (DIS) at HERA have been vital in testing the predictions of perturbative QCD and in the determination of the parton densities of the proton. The recent ZEUS results cover five orders of magnitude in Q^2 and in the Bjorken scaling variable, x [1, 2]. The same cannot, however, be said for the measurement of the longitudinal proton structure function, F_L, which has not been directly measured at HERA. F_L is directly sensitive to scaling violations and hence to the gluon content of the proton and is therefore crucial to our understanding of proton structure.

The first direct measurement of F_L at HERA is presented here, based on the data taken during 1996 and 1997 ($35\,\mathrm{pb}^{-1}$). The measurement is made using events with QED initial-state radiation. The emission of a hard photon from the initial-state positron leads to a variation in the centre-of-mass energy (and hence y) for fixed x and Q^2. This property is exploited to measure F_L. This class of events is also used to measure F_2, using a subset of the data taken in 1996 ($3.78\,\mathrm{pb}^{-1}$). In this case, the reduced centre-of-mass energy leads to a lower Q^2 for a given scattering angle.

2 Kinematics and formalism

The kinematics of the DIS process $e(k) + p(P) \rightarrow e(k') + X$ can be described by the negative four-momentum-transfer squared, Q^2, and y, the fraction of the lepton energy transferred to the proton in its rest frame. For the results presented here, Q^2 was reconstructed using the kinematics of the scattered positron, while y was reconstructed using the "sigma" method [3]. The former method must be corrected for the effects of the emission of the initial-state (ISR) photon, while the latter needs no correction. All quantities used in the reconstruction were determined using information from the high-precision uranium-scintillator calorimeter [4]. The ISR photon was detected in a lead-scintillator calorimeter [5] (LUMI-γ) located at $Z = -107\,\mathrm{m}$ and used for the measurement of the luminosity from the rate of the bremsstrahlung process $ep \rightarrow e\gamma p$. The calorimeter used for the detection of the corresponding final-state positron (LUMI-e) is located at $Z = -35\,\mathrm{m}$ and is used, along with a small electromagnetic calorimeter located close to the beampipe at $Z = -44\,\mathrm{m}$ (44m tagger) [6], to reduce the accidental overlap of DIS and photoproduction events with those from the bremsstrahlung process.

In order to compare the measurements from this analysis with those from previous analyses at the nominal positron beam energy, y must be corrected for the effect of the photon emission. A new variable, y_{HERA}, is therefore defined, where $y_{HERA} = y_{\Sigma} \cdot z$. The quantity

z is defined as $z = (E_e - E_\gamma)/E_e$, where E_e is the positron beam energy, 27.5 GeV, and E_γ is the energy of the ISR photon.

Ignoring the contribution from Z^0 exchange, the double-differential cross section for inclusive e^+p scattering is given in terms of the structure functions F_2 and F_L by

$$\frac{\mathrm{d}^2\sigma^{e^+p}}{dxdQ^2} = \frac{2\pi\alpha^2}{xQ^4} Y_+ \left[F_2(x,Q^2) - \frac{y^2}{Y_+} F_L(x,Q^2) \right] (1 + \Delta_r(x,Q^2)), \tag{1}$$

where $Y_\pm = 1 \pm (1-y)^2$ and Δ_r is the radiative correction. This equation can alternatively be written as:

$$\widetilde{\sigma} = \frac{xQ^4}{2\pi\alpha^2 Y_+} \frac{\mathrm{d}^2\sigma^{e^+p}}{dxdQ^2} = \left(\frac{1+\epsilon R}{1+R} \right) F_2 = F_2 - (1-\epsilon) F_L \tag{2}$$

where $R = \frac{F_L}{F_2 - F_L}$ and $\epsilon = \frac{2(1-y)}{1+(1-y)^2}$. $\widetilde{\sigma}$ is referred to as the reduced cross section.

In practice, it is the double-differential or reduced cross section which can be directly measured and not the structure functions themselves. However, it can be seen from (1) that this is simply a linear combination of F_2 and F_L, with the contribution from F_L being suppressed by the y^2/Y_+ term, which is normally small. The value of F_L is also predicted by QCD to be of the order of α_s, meaning that the reduced cross section is dominated by F_2. This also means that F_2 can be extracted by making a minimal assumption about F_L. In order to disentangle the two structure functions within the reduced cross section it is necessary to measure this cross section as a function of y for fixed x and Q^2. This can only be achieved by varying the beam energies, making the measurement of F_L the more challenging technically.

3 Monte Carlo simulation

Monte Carlo (MC) event simulation is used to correct for detector acceptance and smearing effects. The detector simulation is based on the GEANT program [7] and incorporates the best understanding of the detector, the trigger and test-beam results. Neutral current DIS events with initial-state radiation were simulated using the HERACLES 4.5.2 program [8] interfaced to LEPTO 6.5 [9] by DJANGO6 2.4 [10]. HERACLES is capable of simulating initial- and final-state radiation, and takes account of vertex and propagator corrections. The hadronic final state was simulated using the colour-dipole model CDM-BGF including all leading-order QCD diagrams as implemented in ARIADNE 4.08 [11] for the QCD cascade and JETSET 7.4 [12] for the hadronisation. The ARIADNE model provides the best description of the observed DIS non-diffractive hadronic final state. Diffractive events with a large rapidity gap as observed in the data can also be simulated by ARIADNE, when interfaced to the RAPGAP 2.06/26 program [13]. The latter

assumes that the struck quark belongs to a colourless state having only a small fraction of the proton's momentum. The diffractive and non-diffractive samples were mixed as a function of y_{HERA} and $z \cdot Q^2$ using the $\eta_{\max}$ distribution in the data, where $\eta_{\max}$ is the pseudorapidity of the most forward energy deposit with more than 400 MeV. The ALLM97 [14] parameterisation of F_2 was used in the simulations. ALLM97 uses a Regge-motivated approach based on all available F_2 measurements, including those made in the region of very low Q^2. Only events containing an ISR photon with energy greater than 3 GeV were generated. In all the MC samples $F_L = 0$.

The vertex distribution used in the simulation was taken from DIS events having both scattered positrons and hadrons well reconstructed by the central tracking detector (CTD) [15]. The vertex-finding efficiency is well described by the MC simulation.

4 Event selection

The event sample used here was analysed in a similar manner to the most recently published ZEUS F_2 analysis [1]. The only important difference is in the requirement placed on $\delta = \sum_i (E_i - P_{Z,i})$, where the sum runs over all the energy deposits from the hadronic system and the final-state positron. In a well-contained DIS event in which no ISR photon has been emitted, $\delta \approx 2E_e$. In this analysis, the ISR photon must also be included to satisfy this condition. Therefore, an additional variable, $\delta_{\rm TOT} = \delta + 2E_\gamma$ was defined. Both δ and $\delta_{\rm TOT}$ were used in the event selection.

Events which contain an ISR photon were selected by requiring the energy in the LUMI-γ to be greater than 6 GeV. Requirements were also placed on any energy deposits in the LUMI-e of $E_{\rm LUMI-e} < 2$ GeV and in the 44 m tagger of no more than 10 to 18 GeV, depending on the run conditions. In the F_2 analysis an additional requirement of $\delta > 20$ GeV was made, while in the F_L analysis, this requirement was tightened to $\delta > 22$ GeV. In the 1996 data, the requirement $48 < \delta_{\rm TOT} < 60$ GeV was applied, while in 1997 it was loosened to $46 < \delta_{\rm TOT} < 60$ GeV in order to account for the effect of an additional filter which was placed in front of the LUMI-γ during 1997 data-taking.

4.1 Background estimation

The most significant source of background comes from bremsstrahlung overlays. This contribution was estimated using events that had been accepted online by a trigger for DIS events with a δ cut that was lower than normal. These events were then combined randomly with bremsstrahlung events, creating a "fake" bremsstrahlung-overlay sample.

This overlay sample was normalised to the signal sample for $\delta_{TOT} > 62\,\text{GeV}$. The normalised sample was then used to subtract the overlay contribution in the signal region. It was assumed that any photoproduction events in the signal sample were also accounted for by the subtraction of the overlay sample.

A comparison of the full 1996-97 dataset with the MC samples described in Section 3 and the normalised "fake" bremsstrahlung overlay sample is shown in Fig. 1. The agreement between data and MC is good.

5 Measurement of F_2

Figure 2 shows the range in which the F_2 results from this analysis will be presented ($0.2 < Q^2 < 28.8\,\text{GeV}^2$ and $0.003 < y < 0.6$). The value of F_2 at fixed (y, Q^2) within a bin was obtained from the ratio of the number of observed events, after the subtraction of the bremsstrahling-overlay events, to the number of events predicted from the MC simulation in that bin, multiplied by the value of F_2 predicted by ALLM97. The uncertainty on the normalisation of the bremsstrahlung-overlay sample was accounted for in the systematic uncertainties. The effect of F_L was corrected for using the next-to-leading-order (NLO) ZEUS QCD fit of F_2 [16]. No correction was made in the two lowest Q^2 bins, as the effect of F_L is expected to be much smaller than the statistical uncertainties in these bins.

5.1 Binning and resolution

The electron method used for the Q^2 reconstruction had a resolution of $\sim 10\%$, while the sigma method used for y had a resolution of between 20% and 40% and a systematic shift of up to -10%. The choice of bins was determined by the resolutions of the kinematic variables, ensuring sufficient statistics, adequate acceptances ($> 20\%$) and purities ($> 30\%$) in all bins.

5.2 Systematic uncertainties

A total of 18 systematic checks were performed, covering: DIS event selection; the measurement of the ISR photon; the MC simulation of the ISR photon and the diffractive contribution; and the parameters of the sample of bremsstrahlung-overlay background. Of these 18 checks, the most significant sources of uncertainty were: the variation of the positron-energy selection requirement by $\pm 1\,\text{GeV}$; the variation of the hadronic energy scale by its uncertainty ($\pm 2\%$); removing the requirement on the LUMI electron energy;

and increasing the requirement on δ by 2 GeV in each (y, Q^2) bin. The systematic uncertainty is only significantly larger than the statistical uncertainty at low x (high y). The systematic uncertainties were added in quadrature separately for the positive and negative deviations from the nominal values of F_2 in each $(y - Q^2)$ bin.

5.3 Results

The F_2 measurements are shown in Fig. 3 as a function of x at different values of Q^2. They are presented together with the most recently published F_2 measurements [1], those at low Q^2 [2] and those with a vertex shifted with respect to the nominal vertex by 70 cm [17], another technique that allows lower Q^2 events than normal to be measured. The four data sets are in good agreement in the region of overlap, completing the coverage of the x-Q^2 plane at low Q^2, as seen in Fig. 2. The current analysis extends the measurement of F_2 into regions of the $x - Q^2$ plane not previously explored by ZEUS. The consistency of the results shows that ISR events detected in the ZEUS detector are well-understood, giving confidence that they can also be used to measure F_L. The measurements from this analysis also extend to lower values of Q^2 than in the previous $F_2(ISR)$ analysis [18]. The results are compared to the predictions of the ZEUS NLO QCD fit for $Q^2 \geq 1.3\,\mathrm{GeV}^2$ and to the predictions of ALLM97 over the whole Q^2 range. Both predictions provide a good description of the data.

6 Measurement of F_L

In order to measure F_L the quantity δ_{F_L} is used, which is defined as

$$\delta_{F_L} = \frac{1 + \epsilon R}{1 + R} \tag{3}$$

and is equivalent to the ratio $\widetilde{\sigma}\ (F_L \neq 0)/\ \widetilde{\sigma}\ (F_L = 0)$ (see (2)). In practice, δ_R, the ratio of the number of background-subtracted data events to the number of MC events as a function of y, is measured at the detector level. The shapes of the data and MC distributions which make up this ratio are both controlled by the e^+p cross section, as defined in (1). The δ_R distribution is then fitted using the function $\delta_R = N_{\mathrm{fit}} \cdot \delta^S_{F_L}$, where N_{fit} is a free parameter of the fit. $\delta^S_{F_L}$ has the same functional form as δ_{F_L}, except that ϵ has been replaced by ϵ_S, where $\epsilon_S = \frac{2(1-y')}{1+(1-y')^2}$ and $y' = S_y \cdot y$, with S_y being a correction factor determined from MC studies. In the fit function, R is replaced by $F_L/(F_2 - F_L)$, with F_L as a free parameter of the fit and F_2 fixed. The value of F_2 is measured using the procedure described in Section 5, but without the F_L correction being applied.

6.1 Systematic uncertainties

The sources of systematic uncertainty which were considered for the F_L measurement are the same as those considered for F_2. In addition, the range of $y_{\rm HERA}$ used was also varied. It was found in this case that the systematic uncertainty was completely dominated by the hadronic energy scale uncertainty. As a result the systematic uncertainty on F_L was estimated solely from this source.

6.2 Results

The measurement of F_L is made in a single bin defined by $1 < Q^2 < 30\,\mathrm{GeV}^2$ and $0.11 < y_{\rm HERA} < 0.23$. This determines the (x, Q^2) value at which F_L is being measured. The values of x and Q^2 are taken to be the logarithmic bin centres. The ratio, δ_R, measured as a function of y in this bin is shown in Fig. 4, along with the result of the fit. Figure 5 shows the value of F_2 measured in this bin, along with the most recently published ZEUS F_2 measurements and the predictions of ALLM97 and the ZEUS NLO QCD fit. The two sets of measurements are consistent with each other and with the theoretical predictions. The value of F_L determined from the fit is shown in Fig. 6. It is compared to the predictions for F_2 and F_L from the ZEUS NLO QCD fit. Although the measurement is not currently very precise and cannot distinguish between $F_L = 0$ and $F_L = F_2$, the value is clearly consistent with the expectations of perturbative QCD. The correction to F_L from the measured F_2 used in the extraction described in Section 6 is of the order of 10^{-5} because of the smallness of the y^2/Y_+ factor discussed in Section 2.

7 Summary

Events with hard initial-state radiation have been used to make the first direct measurement of the F_L structure function at HERA, as well as to measure the F_2 structure function in the overlap region between the ZEUS low-Q^2 and nominal-vertex data. Although the measurement of F_L is not very precise, it is clearly consistent with the expectations of perturbative QCD. In the case of the F_2 measurements, good agreement is achieved in the region of overlap and the data extend the ZEUS measurement of F_2 into a previously unexplored region. In order to achieve F_L measurements with comparable accuracy to the HERA F_2 measurements, reduced proton energy running would be required.

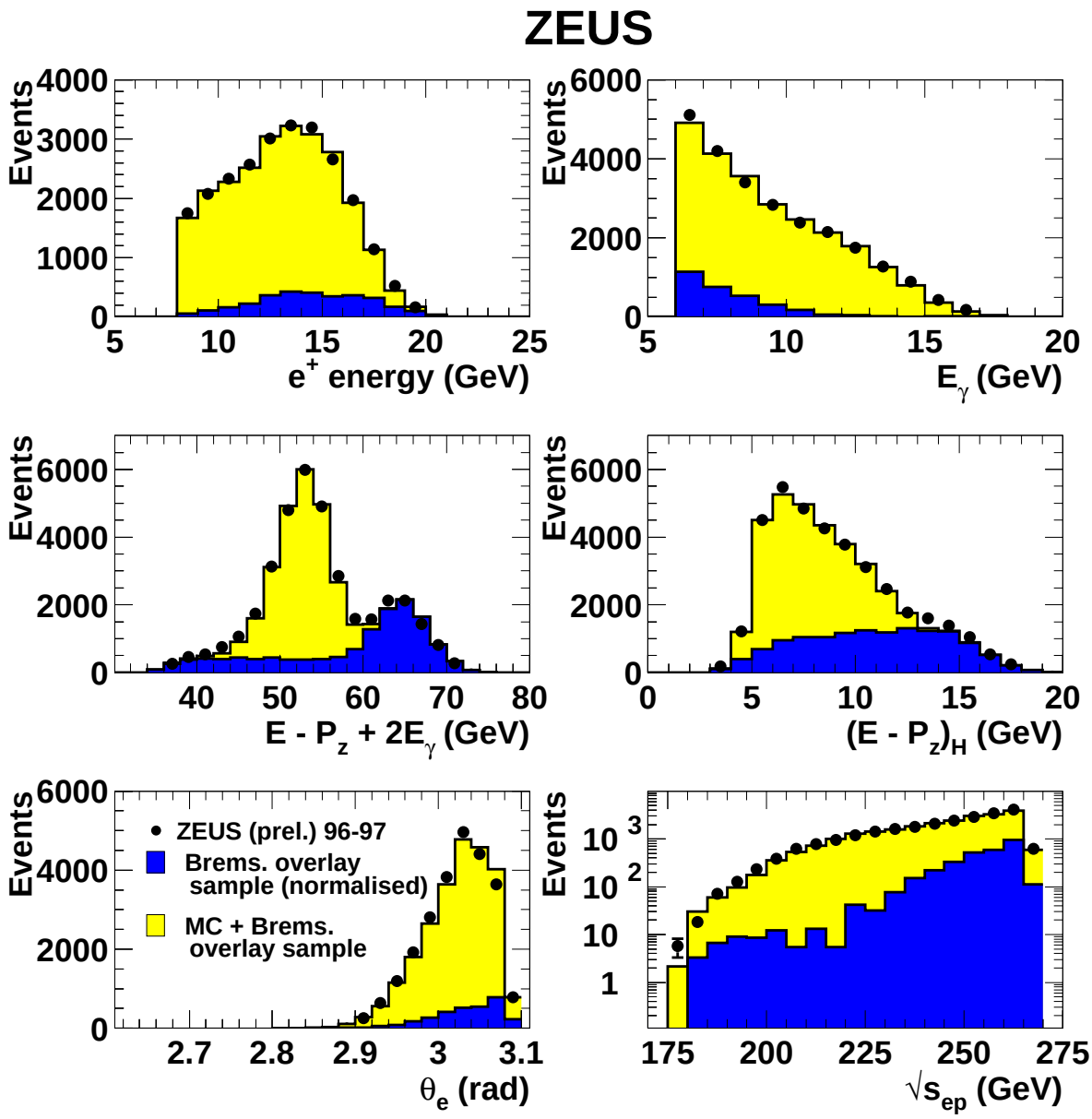

Figure 1: *A comparison of detector-level distributions in data, Monte Carlo and the normalised "fake" bremsstrahlung-overlay sample. The Monte Carlo histograms are normalised to luminosity and then mixed with the normalised bremsstrahlung-overlay histograms. The latter are also shown separately.*

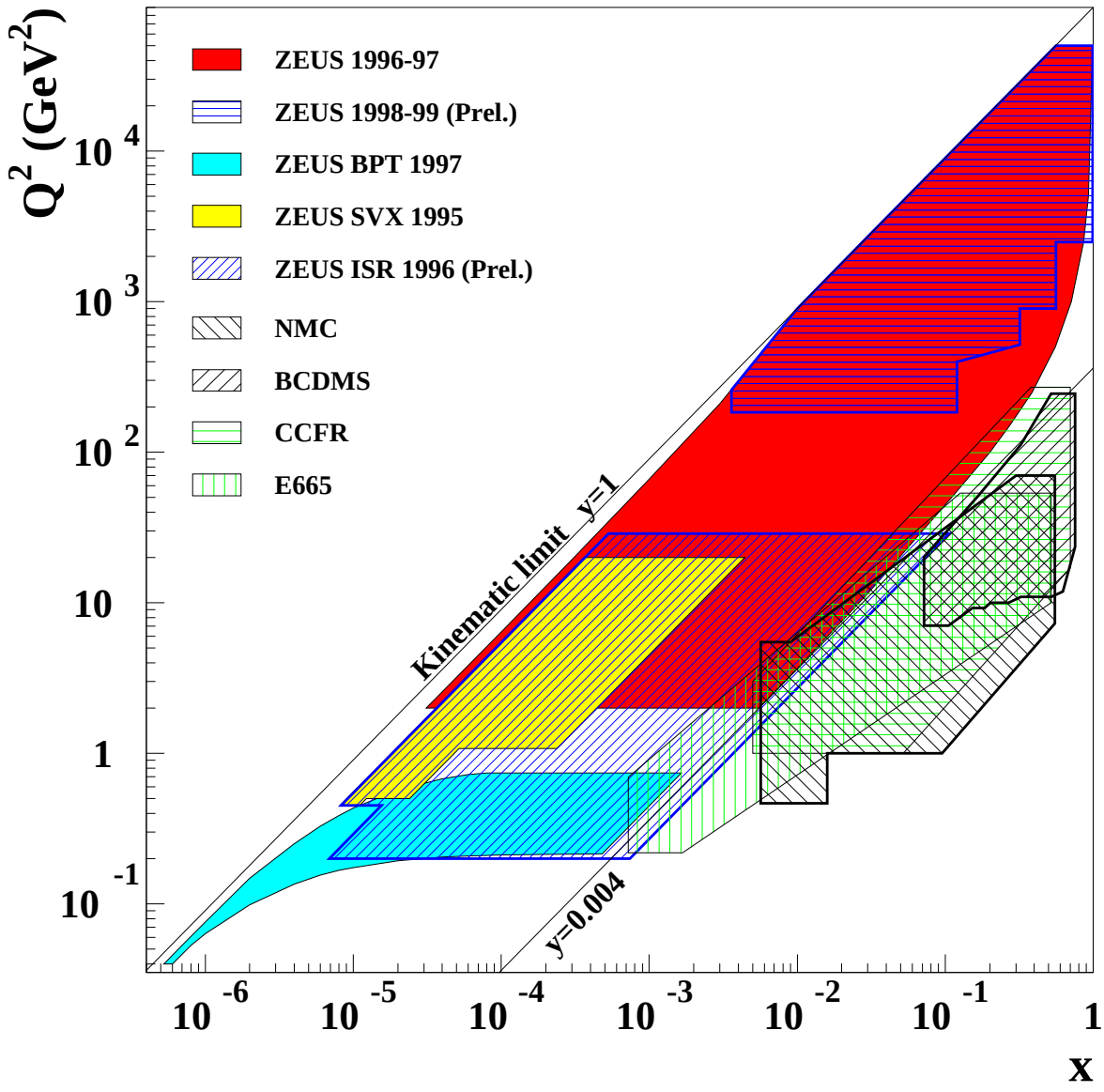

Figure 2: *The kinematic plane in terms of x and Q^2 for deep inelastic scattering. The regions in which different measurements have been made are shown, including the region for this analysis.*

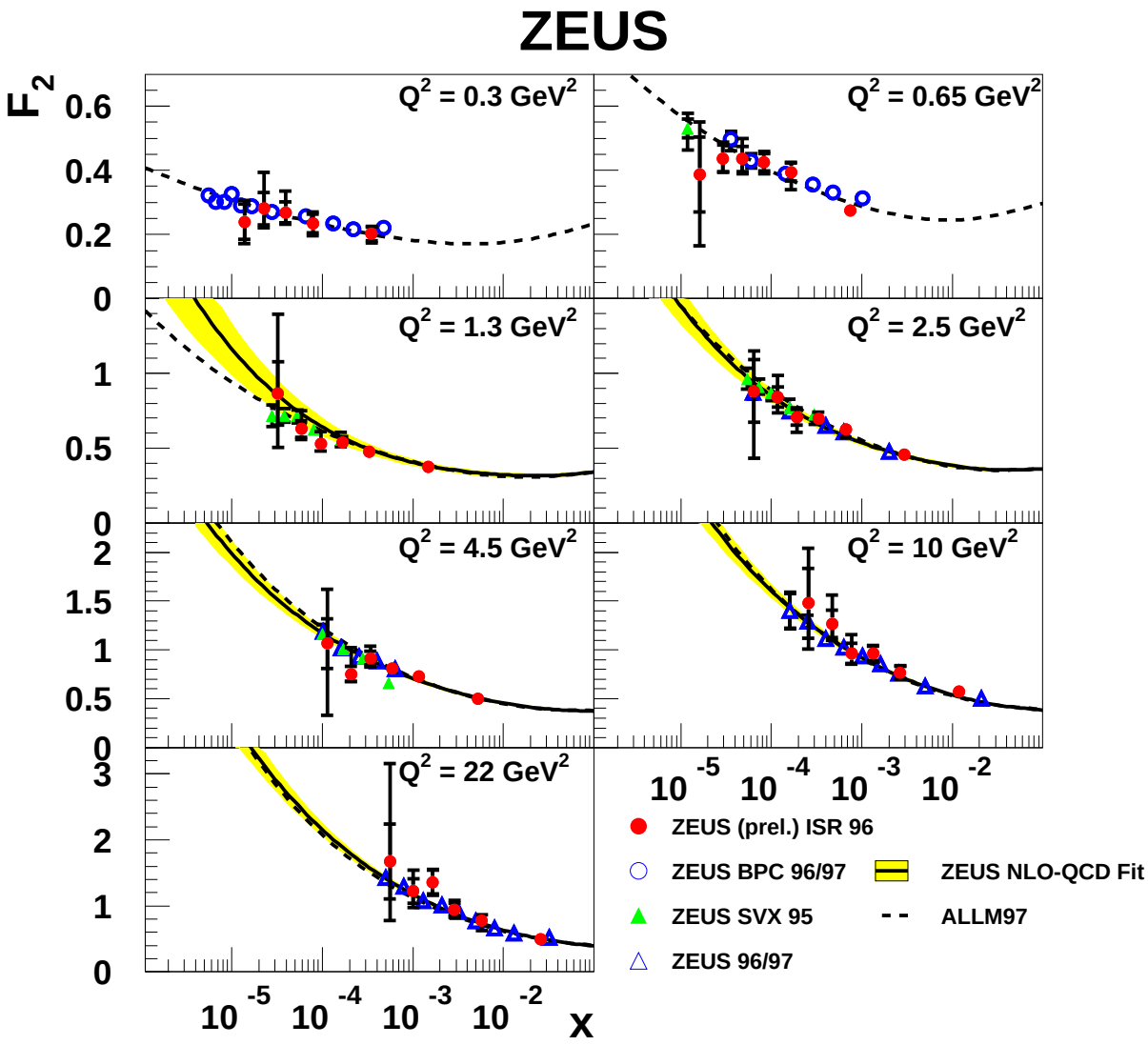

Figure 3: *The results for F_2 (points) versus x for fixed Q^2. The results from this analysis are shown together with previously published ZEUS results. The inner error bars show the statistical uncertainties, while the outer ones show the statistical and systematic uncertainties added in quadrature. The yellow bands show the predictions from the ZEUS NLO QCD fit, while the dashed curves show the predictions from ALLM97.*

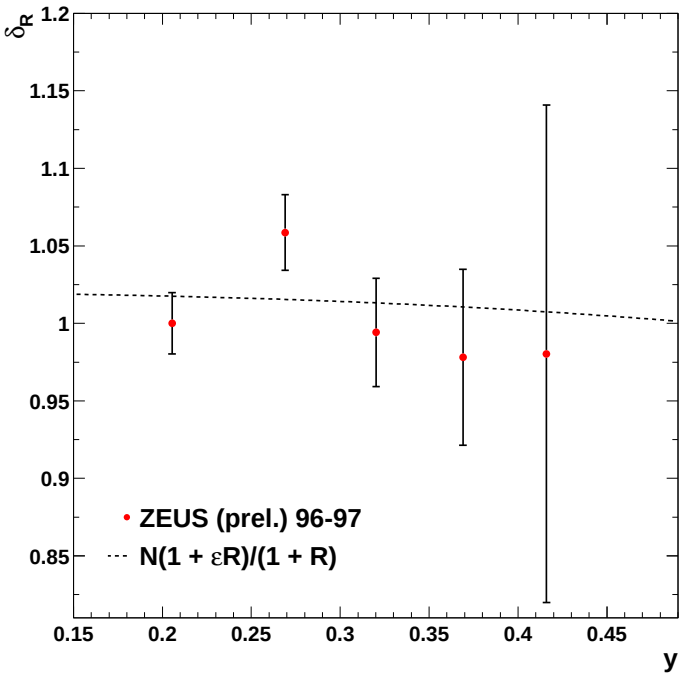

Figure 4: *The ratio of background-subtracted data events to MC events at the detector level as a function of y (points). The error bars show the statistical uncertainties only. The dashed curve is the function fitted to these points to determine the value of F_L.*

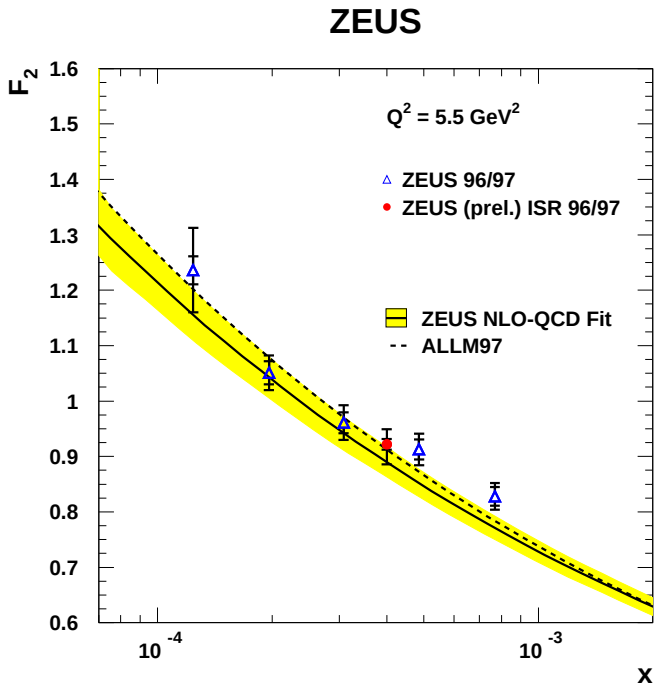

Figure 5: *The results for F_2 (points) versus x for $Q^2 = 5.5\,GeV^2$. The result from the F_L analysis is shown together with the previously published ZEUS results. The inner error bars show the statistical uncertainties, while the outer ones show the statistical and systematic uncertainties added in quadrature. The yellow band shows the prediction from the ZEUS NLO QCD fit, while the dashed curve shows the prediction from ALLM97.*

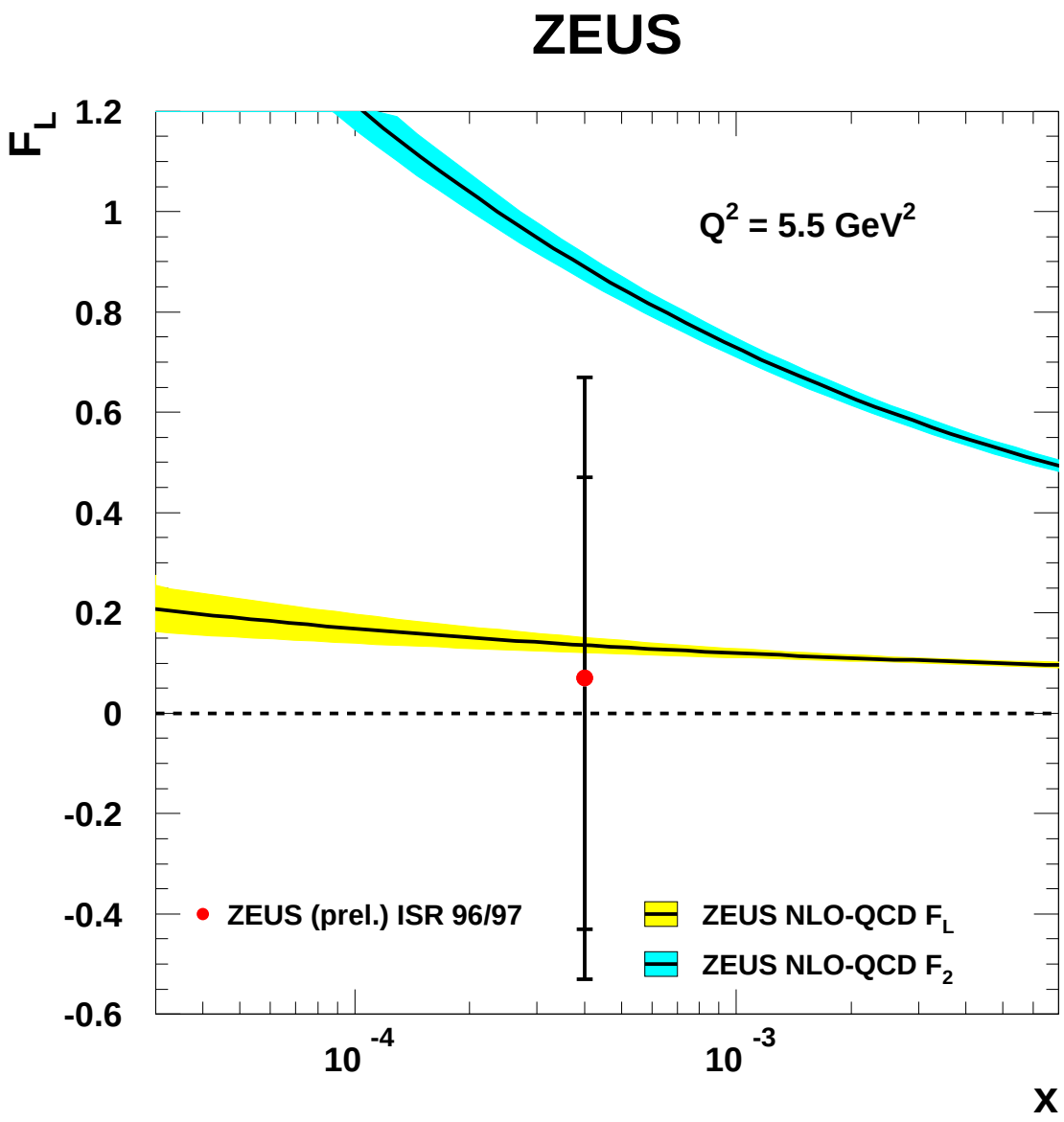

Figure 6: *The result for F_L (point) plotted for $x = 4 \times 10^{-4}$ and $Q^2 = 5.5\ GeV^2$. The inner error bars show the statistical uncertainties, while the outer ones show the statistical and systematic uncertainties added in quadrature. The yellow band shows the prediction for F_L from the ZEUS NLO QCD fit, while the light blue band shows the prediction for F_2, which is the maximum possible value of F_L ($R = \infty$).*

References

[1] ZEUS Coll., S. Chekanov et al., Eur. Phys. J. **C 21**, 443 (2001).

[2] ZEUS Coll., J. Breitweg et al., Phys. Lett. **B 487**, 53 (2000).

[3] U. Bassler and G. Bernardi, Nucl. Inst. Meth. **A 361**, 197 (1995).

[4] M. Derrick et al., Nucl. Inst. Meth. **A 309**, 77 (1991);
A. Andresen et al., Nucl. Inst. Meth. **A 309**, 101 (1991);
A. Caldwell et al., Nucl. Inst. Meth. **A 321**, 356 (1992);
A. Bernstein et al., Nucl. Inst. Meth. **A 336**, 23 (1993).

[5] J. Andruszków et al., Preprint DESY-92-066, DESY, 1992;
ZEUS Coll., M. Derrick et al., Z. Phys. **C 63**, 391 (1994);
J. Andruszków et al., Acta Phys. Pol. **B 32**, 2025 (2001).

[6] ZEUS Coll., J. Breitweg et al., Eur. Phys. J. **C 14**, 213 (2000).

[7] R. Brun et al., GEANT3, Technical Report CERN-DD/EE/84-1, CERN, 1987.

[8] A. Kwiatkowski, H. Spiesberger and H.-J. Möhring, Comp. Phys. Comm. **69**, 155 (1992). Also in *Proc. Workshop Physics at HERA*, 1991, DESY, Hamburg.

[9] G. Ingelman, A. Edin and J. Rathsman, Comp. Phys. Comm. **101**, 108 (1997).

[10] K. Charchula, G.A. Schuler and H. Spiesberger, Comp. Phys. Comm. **81**, 381 (1994).

[11] L. Lönnblad, Comp. Phys. Comm. **71**, 15 (1992).

[12] T. Sjöstrand, Comp. Phys. Comm. **82**, 74 (1994).

[13] H. Jung, Comp. Phys. Comm. **86**, 147 (1995).

[14] H. Abramowicz and A. Levy, Preprint DESY-97-251 (hep-ph/9712415), DESY, 1997.

[15] N. Harnew et al., Nucl. Inst. Meth. **A 279**, 290 (1989);
B. Foster et al., Nucl. Phys. Proc. Suppl. **B 32**, 181 (1993);
B. Foster et al., Nucl. Inst. Meth. **A 338**, 254 (1994).

[16] ZEUS Coll., S. Chekanov et al., Preprint DESY-02-105, 2002.

[17] ZEUS Coll., J. Breitweg et al., Eur. Phys. J. **C 7**, 609 (1999).

[18] ZEUS Coll., M. Derrick et al., Z. Phys. **C 69**, 607 (1996).